# Second-Order Closure PBL Model with New Third-Order Moments: Comparison with LES Data

V. M. CANUTO, F. MINOTTI, C. RONCHI,* AND R. M. YPMA

*NASA/Goddard Institute for Space Studies, New York, New York*

O. ZEMAN

*Center for Turbulence Research, Stanford University, Stanford, California*

(Manuscript received 21 December 1992, in final form 15 October 1993)

ABSTRACT

This paper contains two parts. In the first part, a new set of diagnostic equations is derived for the third-order moments for a buoyancy-driven flow, by exact inversion of the prognostic equations for the third-order moment equations in the stationary case. The third-order moments exhibit a universal structure: they all are a linear combination of the derivatives of all the second-order moments, $\overline{w^2}$, $\overline{w\theta}$, $\overline{\theta^2}$, and $\overline{q^2}$. Each term of the sum contains a turbulent diffusivity $D_t$, which also exhibits a universal structure of the form $D_t = a\nu_t + b\overline{w\theta}$. Since the sign of the convective flux changes depending on stable or unstable stratification, $D_t$ varies according to the type of stratification. Here $\nu_t \sim wl$ ($l$ is a mixing length and $w$ is an rms velocity) represents the "mechanical" part, while the "buoyancy" part is represented by the convective flux $w\theta$. The quantities $a$ and $b$ are functions of the variable $(N\tau)^2$, where $N^2 = g\alpha\partial\Theta/\partial z$ and $\tau$ is the turbulence time scale. The new expressions for the third-order moments generalize those of Zeman and Lumley, which were subsequently adopted by Sun and Ogura, Chen and Cotton, and Finger and Schmidt in their treatments of the convective boundary layer.

In the second part, the new expressions for the third-order moments are used to solve the ensemble average equations describing a purely convective boundary layer heated from below at a constant rate. The computed second- and third-order moments are then compared with the corresponding LES results, most of which are obtained by running a new LES code, and part of which are taken from published results. The ensemble average results compare favorably with the LES data.

## 1. Introduction

The first detailed observations in the atmospheric convective boundary layer (CBL) were made at Wangara (Clarke et al. 1971). In particular, the Wangara day 33 yielded almost a day of data that, with the exception of the early morning, were devoid of effects due to shear. At about the same time, Willis and Deardorff (1974) performed laboratory measurements with water to simulate a purely CBL with zero wind. The CBL was deemed to consist of (i) a well-mixed bulk region with vigorous turbulent activity and almost uniform mean potential temperature profile and (ii) a capping inversion whose strength depended mainly on the initial conditions and the CBL history of the surface heat flux. The negative heat flux produced by the entrainment of warmer air from above into the mixed bulk region of the CBL was maintained by the flux of turbulence kinetic energy.

The first models of the CBL were the so-called slab or one-layer models. With phenomenological assumptions rooted on observations, these models were successfully employed for the prediction of the inversion rise in air pollution meteorology (e.g., see Zeman and Tennekes 1977). At the same time, the second-order closure- (SOC) type models were incapable of reproducing certain critical features of the CBL, such as the magnitude of the inversion heat flux and therefore the CBL growth. This deficiency was traced to the downgradient model used to evaluate the third-order moments that appear in the ensemble average equations describing the second-order moments (Wyngaard and Cote 1975; Zeman 1975). For example, while the observed vertical flux of the turbulent kinetic energy ($F_{KE} = \frac{1}{2}\overline{q^2 w}$) is positive throughout the whole CBL, the downgradient approximation yields a negative value in the lower half of the layer. As a consequence, the divergence of $F_{KE}$ near the inversion layer, which provides the energy to maintain the entrainment process, was underestimated, thus resulting in an unrealistically low inversion heat flux. Zeman (1975), Zeman and

* Current affiliation: ENEA, Italy.

*Corresponding author address:* Dr. V. M. Canuto, NASA/Goddard Institute for Space Studies, 2880 Broadway, New York, NY 10025.

Lumley (1976, hereafter referred to as ZL), and Andre et al. (1976) showed that by including the buoyancy terms in the equations for the third-order moments, one could obtain the correct magnitude and sign of the transport terms. ZL proposed algebraic expressions for the third-order moments by invoking (i) stationarity, (ii) zero fourth-order cumulants, and (iii) eddy and viscous damping. To obtain a manageable set of equations, which would not require complex mathematical manipulations such as tensor inversion, ZL had to further drastically reduce the full expressions for the third-order moments. Specifically, they neglected the contriution of mean temperature gradient (justified within the mixed region), and the explicit dependence on buoyancy of $wu^2$ (the vertical flux of the horizontal components of the turbulent kinetic energy). The eddy diffusivities were assumed to have a qualitatively correct form but were not derived from the equations themselves [see Eq. (38) of ZL]. In spite of these approximations, the predicted third-order moments were found to be in broad agreement with observations. Since the CBL predictions of the ZL model were superior to those of the early first-order or simple downgradient SOC models, the ZL third-order moments were subsequently adopted without further modifications by Sun and Ogura (1980), Chen and Cotton (1983), and Finger and Schmidt (1986).

The ZL model has several drawbacks, however. For example, the predicted inversion interface was rather diffuse, and quantities such as the temperature variance near the inversion layer did not match the observations, which indicate a pronounced narrow peak. Furthermore, the model yielded negative values of $F_{\mathrm{KE}}$ near the ground, and the horizontal rms velocities were underpredicted. In retrospect, it can be said that many of the imperfections in the ZL model were attributable to the crude model for the third-order moments as well as to the equation for $\epsilon$, the rate of dissipation of kinetic energy, which was unnecessarily complex, and to incompatible boundary conditions near the ground.

It must be noted that Andre et al. (1976) retained the full third-order moment prognostic equations but, to obtain realizable second-order moments in the absence of eddy damping terms, they were forced to clip the third-order moments.

## 2. Model problem and basic equations

In order to test the ensemble average model with the new third-order moments, we study the time evolution of an unsheared boundary layer heated from below at a constant and uniform rate, switched on at the initial time. The physical parameters and initial and boundary conditions were chosen to simulate Deardorff's experiment in its revised version (Deardorff and Willis 1985). The dynamical equations governing the mean temperature $\Theta$, the convective flux $\overline{w\theta}$, the temperature variance $\overline{\theta^2}$, and the vertical and horizontal kinetic energies $\frac{1}{2}\overline{w^2}$ and $\overline{u^2}$ are well known (ZL; Sun and Ogura 1980; Bougeault 1981; Finger and Schmidt 1986):

$$\frac{\partial \Theta}{\partial t} = -\frac{\partial}{\partial z}\overline{w\theta} \tag{1}$$

$$\frac{\partial}{\partial t}\overline{w\theta} + \frac{\partial}{\partial z}\overline{\theta w^2} = \overline{\beta w^2} + \lambda\overline{\theta^2} - \Pi_3^\theta \tag{2}$$

$$\frac{\partial \overline{\theta^2}}{\partial t} + \frac{\partial}{\partial z}\overline{w\theta^2} = 2\beta\overline{w\theta} - 2\epsilon_\theta \tag{3}$$

$$\frac{\partial \overline{w^2}}{\partial t} + \frac{\partial}{\partial z}\overline{w^3} = 2\lambda\overline{w\theta} - \Pi_{33} - \frac{2}{3}\epsilon \tag{4}$$

$$\frac{\partial \overline{u^2}}{\partial t} + \frac{\partial}{\partial z}\left(\frac{1}{2}\overline{q^2 w} - \frac{1}{2}\overline{w^3}\right) = \frac{1}{2}\Pi_{33} - \frac{2}{3}\epsilon. \tag{5}$$

Here, $\Theta$ is the mean potential temperature, $\beta = -\partial\Theta/\partial z$, $\lambda = g\alpha$, $g$ is the acceleration due to gravity, and $\alpha$ is the volume expansion coefficient. To solve these equations, one needs three ingredients: the pressure correlations $\Pi$, the dissipation rates $\epsilon$ and $\epsilon_\theta$, and the third-order moments, which we shall discuss in turn.

The pressure–temperature and the pressure–velocity correlations, defined as

$$\Pi_3^\theta \equiv \overline{\theta\, \partial p/\partial z} \tag{6}$$

$$\Pi_{33} \equiv 2\overline{w\, \partial p/\partial z}\,, \tag{7}$$

are modeled, in the absence of mean shear, with the following expressions (Zeman and Lumley 1979; Shih and Lumley 1985; Shih and Shabbir 1992):

$$\Pi_3^\theta = 2c_6\tau_p^{-1}\overline{w\theta} + c_7\lambda\overline{\theta^2} \tag{10}$$

$$\Pi^{33} = 2c_4\tau_p^{-1}\left(\overline{w^2} - \frac{1}{3}\overline{q^2}\right) + \frac{4}{3}c_5\lambda\overline{w\theta} + 2\frac{\partial}{\partial z}\overline{pw}. \tag{11}$$

The return-to-isotropy time scale $\tau_p$ is usually assumed to be equal to $\tau = 2e/\epsilon$, where $e$ is the turbulent kinetic energy $e = \overline{u^2} + \frac{1}{2}\overline{w^2}$. However, from Weinstock's work (1987) one can deduce that in the presence of stable stratification, the appropriate time scale $\tau_p$ is given by

$$\tau_p = \tau(1 + C_w N^2\tau^2)^{-1}, \tag{12}$$

where $C_w = 0.04$, if $N^2 > 0$, and $C_w = 0$, if $N^2 \leq 0$. Here $N$ is the Brunt–Väisälä frequency $N^2 = g\alpha\partial\Theta/\partial z$. A similar result also follows from quite an independent analysis of a stably stratified turbulence recently developed by two of the authors (Canuto and Minotti 1993). We have found that the use of Eq. (12) considerably improves the behavior of all quantities near the inversion layer, in particular $\overline{u^2}$, which otherwise would decrease too fast near the inversion layer. The results shown in this paper were all obtained using Eq. (12). Finally, using Lumley's suggestion (1978), the term $\overline{pw}$ in (11) is modeled as $-aq^2w$, where the constant $a$ is discussed in section 8.

The rate of dissipation of turbulent kinetic energy $\epsilon$ is described by the following dynamic equation:

$$\frac{\partial \epsilon}{\partial t} + \frac{\partial}{\partial z}\overline{w\epsilon} = 2a_1\tau^{-1}\lambda\overline{w\theta} - a_2\epsilon\tau^{-1} + a_3N\tau^{-1}\overline{w^2} \quad (13)$$

with

$$\overline{\epsilon w} = -\frac{3}{2}A_0\tau(\overline{w^2} + A_0\tau\lambda\overline{w\theta})\frac{\partial \epsilon}{\partial z}. \quad (14)$$

Here, $a_3 = 0.3$ if $N^2 > 0$ and $a_3 = 0$ otherwise and $\tau = 2e/\epsilon$. Equation (13) is different from the usual equation for $\epsilon$ used in the well-known $K-\epsilon$ model (Speziale 1991), from the dynamic equation employed by ZL, and from the relation used by Sun and Ogura (1980), Chen and Cotton (1983), and Finger and Schmidt (1986). Specifically, in the latter works, the authors employ the local version of (13); namely,

$$\epsilon = \frac{e^{3/2}}{\Lambda}, \quad (15)$$

where the mixing length $\Lambda$ is described with phenomenological expressions of the type suggested by Blakadar (Sun and Ogura 1980). Zeman and Lumley kept the nonlocal character of (13) but employed a considerably more complex equation. Finally, in the $K-\epsilon$ model, even when applied to buoyant flows, the third-order moment $\overline{w\epsilon}$ does not contain the convective flux $\overline{w\theta}$, $\overline{w\epsilon}$ being taken to be proportional to the "mechanical" diffusivity $\tau\overline{w^2}$, rather than to the sum that appears in (14) and is more physically justified in the light of the general structure for the third-order moments to be discussed in the following.

Equation (13) contains a new term, the last one. Its appearance is based on the phenomenological argument that the vertical excursion (say $l_w$) of the eddies is limited by the stable stratification so that the vertical kinetic energy ($w^2$) should be of the same order of the potential energy $N^2l_w^2$. This leads to an enhancement of $\epsilon \propto q^3/l_w$ [see also the related argument in Zeman and Tennekees (1977)]. The contribution is also important to maintain quasi stationarity in homogeneous, strati2fied turbulence, as was verified by one of the authors (OZ) by comparing the model with DNS data of stratified shear turbulence (Holt et al. 1992). Note also that for negligible heat flux and neglecting the left-hand side, Eq. (13) implies $\epsilon \propto N\overline{w^2}$, which is equivalent to $N^2l_w^2/w^2 = O(1)$.

Finally, $\epsilon_\theta$ will be modeled as suggested by Andre et al. (1982):

$$\epsilon_\theta = c_2\frac{\epsilon}{e}\overline{\theta^2}. \quad (16)$$

## 3. Dynamic equations for the third-order moments

The dynamic equations for the third-order moments $\overline{\theta w^2}$, $\overline{w\theta^2}$, $\overline{w^3}$, and $\overline{q^2w}$ needed in Eqs. (2)–(5) can be derived from the Navier–Stokes equations (Andre et al. 1982; Canuto 1992). These equations contain fourth-order moments and pressure and dissipation terms that need to be modeled. The fourth-order mome2nts are taken as products of second-order moments by assuming quasi normality (Hanjalic and Launder 1972, 1976). The pressure terms are split into diagonal and trace-free parts. The former are modeled as a source, while the latter are treated in analogy with the pressure terms (6) and (7). They are divided into a slow part modeled via a return-to-isotropy expression and a rapid part taken to be proportional to the anisotropic production terms. Finally, the dissipation terms are all written in terms of the dissipation of turbulent kinetic energy $\epsilon$ with the assumption of isotropic dissipation scales. The results are [for a detailed derivation see Zeman and Lumley (1979); Bougeault (1981); Andre et al. (1982); Bougeault and Andre (1986); Canuto (1992)]:

$$\left(\frac{\partial}{\partial t} + \tau_3^{-1}\right)\overline{w^2\theta} = \beta\overline{w^3} - \overline{w\theta}\frac{\partial}{\partial z}\overline{w^2} + 2\left(1 - \frac{2}{3}c_{11}\right) \times \lambda\overline{w^2\theta} - 2\overline{w^2}\frac{\partial}{\partial z}\overline{w\theta} + \tau^{-1}c_*\overline{q^2\theta} \quad (17)$$

$$\left(\frac{\partial}{\partial t} + \tau_3^{-1} + 2\tau_\theta^{-1}\right)\overline{w\theta^2} = 2\beta\overline{w^2\theta} - 2\overline{w\theta}\frac{\partial}{\partial z}\overline{w\theta} - \overline{w^2}\frac{\partial}{\partial z}\overline{\theta^2} + (1 - c_{11})\lambda\overline{\theta^3} \quad (18)$$

$$\left(\frac{\partial}{\partial t} + \tau_3^{-1}\right)\overline{w^3} = -3\overline{w^2}\frac{\partial}{\partial z}\overline{w^2} + 3(1 - c_{11})\lambda\overline{w^2\theta} - 2\tau^{-1}\overline{q^2w} \quad (19)$$

$$\left(\frac{\partial}{\partial t} + \tau_3^{-1} + \frac{10}{3}\tau^{-1}\right)\overline{q^2w} = -\left(2\overline{w^2}\frac{\partial}{\partial z}\overline{w^2} + \overline{w^2}\frac{\partial}{\partial z}\overline{q^2\theta}\right) + \lambda(1 - c_{11})(2\overline{w^2\theta} + \overline{q^2\theta}) \quad (20)$$

$$\left(\frac{\partial}{\partial t} + \tau_3^{-1}\right)\overline{q^2\theta} = \beta\overline{q^2w} + 2\lambda\overline{w\theta^2} - \left(2\overline{w^2}\frac{\partial}{\partial z}\overline{w\theta} + \overline{w\theta}\frac{\partial}{\partial z}\overline{q^2}\right) + 3c_*\tau^{-1}\overline{q^2\theta} \quad (21)$$

$$\left(\frac{\partial}{\partial t} + \frac{c_{10}}{c_8}\tau_3^{-1}\right)\overline{\theta^3} = 3\beta\overline{w\theta^2} - 3\overline{w\theta}\frac{\partial}{\partial z}\overline{\theta^2}, \quad (22)$$

where $3c_* \equiv 2(c_8 + 3c_9 - c_{10})$, $\tau_\theta = \overline{\theta^2}/\epsilon_\theta$, and $2c_8\tau_3 \equiv \tau$.

## 4. The solution of Eqs. (17)–(22)

If one considers a stationary case, Eqs. (17)–(22) become an algebraic system of equations for the third-order moments, which can be inverted using a symbolic algebra program. The result is

$$\lambda\tau\overline{w^2\theta} = \lambda\tau A_1 \frac{\partial}{\partial z}\overline{w\theta} + A_2 \frac{\partial}{\partial z}\overline{w^2} + (\lambda\tau)^2 A_3 \frac{\partial}{\partial z}\overline{\theta^2} + A_4 \frac{\partial}{\partial z}\overline{q^2} \quad (23)$$

$$\overline{w^3} = \lambda\tau B_1 \frac{\partial}{\partial z}\overline{w\theta} + B_2 \frac{\partial}{\partial z}\overline{w^2} + (\lambda\tau)^2 B_3 \frac{\partial}{\partial z}\overline{\theta^2} + B_4 \frac{\partial}{\partial z}\overline{q^2} \quad (24)$$

$$(\lambda\tau)^2\overline{w\theta^2} = \lambda\tau C_1 \frac{\partial}{\partial z}\overline{w\theta} + C_2 \frac{\partial}{\partial z}\overline{w^2} + (\lambda\tau)^2 C_3 \frac{\partial}{\partial z}\overline{\theta^2} + C_4 \frac{\partial}{\partial z}\overline{q^2} \quad (25)$$

$$\lambda\tau\overline{q^2\theta} = \lambda\tau D_1 \frac{\partial}{\partial z}\overline{w\theta} + D_2 \frac{\partial}{\partial z}\overline{w^2} + (\lambda\tau)^2 D_3 \frac{\partial}{\partial z}\overline{\theta^2} + D_4 \frac{\partial}{\partial z}\overline{q^2} \quad (26)$$

$$\overline{q^2 w} = \lambda\tau E_1 \frac{\partial}{\partial z}\overline{w\theta} + E_2 \frac{\partial}{\partial z}\overline{w^2} + (\lambda\tau)^2 E_3 \frac{\partial}{\partial z}\overline{\theta^2} + E_4 \frac{\partial}{\partial z}\overline{q^2} \quad (27)$$

$$(\lambda\tau)^3\overline{\theta^3} = \lambda\tau F_1 \frac{\partial}{\partial z}\overline{w\theta} + F_2 \frac{\partial}{\partial z}\overline{w^2} + (\lambda\tau)^2 F_3 \frac{\partial}{\partial z}\overline{\theta^2} + F_4 \frac{\partial}{\partial z}\overline{q^2}, \quad (28)$$

where the coefficients in front of the third-order moments have been chosen so that all the left-hand sides of Eqs. (23)–(28) have dimensions of velocity cubed. Several remarks are in order. First, the downgradient approximation is recovered by assuming that

$$A_{2,3,4} = 0, \quad B_{1,3,4} = 0, \quad C_{1,2,4} = 0, \quad D_{2,3,4} = 0, \quad E_{1,2,3} = 0. \quad (29)$$

Second, all the third-order moments exhibit the same structure; namely, they all are a linear combination of the derivatives of all the second-order moments. Third, all the *turbulent* diffusivities $A$, $B$, $C$, $D$, $E$, and $F$ exhibit the same general structure, namely,

$$A_i = A_{i_1}\tau\overline{w^2} + A_{i_2}\lambda\tau^2\overline{w\theta}, \quad (30)$$

and the same holds true for $B, \ldots, F$. The $A_{i_1}$ and $A_{i_2}$ are dimensionless functions of the dimensionless combination $g\alpha\beta\tau^2$ (see appendix). Equation (30) shows that the turbulent diffusivities are contributed by a *mechanical* part $\nu_t \sim lw \sim \tau\overline{w^2}$, where $l$ is a mixing length, which represents the standard form for the turbulent viscosity, plus a *buoyant part* due to the presence of the convective flux $\overline{w\theta}$. It was the inclusion of this latter component that allowed Sun and Ogura (1980) to obtain better agreement with the large eddy simulation (LES) data than with the downgradient approximation (Moeng and Wyngaard 1989). It is important to note that the inclusion of this buoyant contribution is accomplished by ZL using an ad hoc argument suggested by a Lagrangian–statistical description of heat transfer in inhomogeneous turbulence (Lumley et al. 1978) rather than by the solution of the dynamical equations, as we have done here. Irrespective of the derivation, neither Sun and Ogura (1980) nor Finger and Schmidt (1986) have included *all* the second-order moments appearing in (23)–(28). Specifically, all the SOC models thus far have taken

$$A_4 = B_4 = C_2 = C_4 = 0. \quad (31)$$

## 5. Zeman–Lumley third-order moments

For purposes of completeness, we have also solved Eqs. (1)–(5) using the third-order moments of ZL, namely,

$$\overline{w^2\theta} = -\frac{10}{11}K_m \frac{\partial}{\partial z}\overline{w\theta} - \frac{5}{11}\overline{w\theta}\frac{\partial}{\partial z}\overline{w^2} - \frac{3}{4}\lambda\mu\tau K_t \frac{\partial}{\partial z}\overline{\theta^2} \quad (32)$$

$$\overline{w\theta^2} = -K_t \frac{\partial}{\partial z}\overline{\theta^2} \quad (33)$$

$$\overline{w^3} + \frac{2}{3}\overline{pw} = -K_m \frac{\partial}{\partial z}\overline{w^2} - \lambda\mu\tau K_m \frac{\partial}{\partial z}\overline{w\theta} - \frac{3}{4}(\lambda\mu\tau)^2 K_t \frac{\partial}{\partial z}\overline{\theta^2} \quad (34)$$

$$\overline{u^2 w} + \frac{2}{3}\overline{pw} = -\frac{2}{5}K_m \frac{\partial}{\partial z}\overline{u^2}, \quad (35)$$

where

$$K_m = \mu\tau\left(\overline{w^2} + \frac{1}{2}\lambda\mu\tau\overline{w\theta}\right) \quad (36)$$

$$K_t = \tau_c \frac{\overline{w^2} + \lambda\mu\tau\overline{w\theta}}{1 + \frac{1}{6}\tau_c\mu\tau N^2} \quad (37)$$

$$2(2 + c_6)\tau_c = \tau. \quad (38)$$

The constant $\mu$ was taken to be 0.17 rather than the value of 0.31 originally suggested by ZL; this change is probably related to the use of a different equation for the dissipation $\epsilon$.

## 6. LES simulations

The LES was performed with the code described in Nieuwstadt and Brost (1986). The values of the coef-

ficients of the subgrid model and the numerics were unchanged except that the resolved temperature was calculated at the center of the grid volume instead of at the staggered position where the vertical velocity is calculated ($w$ point). This is the same way that Schumann and Mason (Nieuwstadt et al. 1993) calculate their resolved temperature.

The boundary conditions were set as follows. The horizontal conditions satisfy periodicity. At the lower boundary a constant heat flux was prescribed with a value of 6 K cm $s^{-1}$. The vertical velocity $w$ was set to zero at this boundary. For the horizontal velocities, the Monin–Obukhov (M–O) similarity theory was used. At the upper boundary the stress-free boundary condition was used for the horizontal velocities, and the vertical gradient of temperature was fixed to a constant equal to 0.3 K $cm^{-1}$. To avoid reflecting gravity waves, a damping function was applied to the upper 12 grid layers. The damping function had a relaxation time scale of 48 seconds at the highest calculation level and was increased by a factor of 4 at each computation level for the next 11 levels down.

The calculation was performed in a rectangular domain, with horizontal dimensions of 6400 × 6400 $m^2$ and a vertical dimension of 2400 m. The LES was performed on a $(64)^3$ uniform grid. The initial height of the boundary layer was 1680 m, with a time scale $Z_i w_*^{-1}$ of approximately 1100 s. From the initial field the flow was allowed to develop for ten time scales before the statistics were calculated. These statistics were determined over a period of two time scales.

The results obtained are comparable to those of other LES codes as can be seen in Figs. 2–23 [see Nieuwstadt et al. (1993) for a description of these codes]. All second-order moment statistics correspond to total magnitudes (resolved + subgrid). For the third-order moments, only resolved quantities were used. The only systematic difference with other LES is the large fluctuation of temperature above the inversion layer. This is probably due to the values of the coefficients chosen for the damping function.

## 7. Numerical solutions and results

We have solved the system of equations (1)–(5) with either expressions (23)–(28) or (32)–(38), respectively.

The equations were numerically solved using standard finite differences, with centered spatial derivatives and forward time derivatives; we chose a staggered grid where the second-order moments and the dissipation $\epsilon$ are evaluated at the grid boundary, while the mean temperature $\Theta$ and third-order moments are determined at the center of the grid. The solution of the finite-difference system then requires boundary conditions only for the second-order moments and the dissipation $\epsilon$. We have used the expressions suggested by ZL based on the similarity theory:

$$\overline{w\theta} = (\overline{w\theta})_*\left(1 - \frac{z}{Z_i}\right) \tag{39.a}$$

$$\overline{w^2} = 1.25 w_*^2\left(1 - \frac{z}{Z_i}\right)^{2/3}\left(\frac{z}{Z_i}\right)^{2/3} \tag{39.b}$$

$$\overline{u^2} = 0.4 w_*^2 \tag{39.c}$$

$$\overline{\theta^2} = 1.6\theta_*^2\left(1 - \frac{z}{Z_i}\right)^{4/3}\left(\frac{z}{Z_i}\right)^{-2/3} \tag{39.d}$$

$$\epsilon = \lambda(\overline{w\theta})_*\left(1 - \frac{z}{Z_i}\right), \tag{39.e}$$

where $(\overline{w\theta})_*$ is the heat flux at the surface layer, $Z_i$ is the instantaneous value of the position of the minimum of $\overline{w\theta}$, and the convective velocity and temperature scales, $w_*$ and $\theta_*$, respectively, are defined as

$$w_* = [\lambda(\overline{w\theta}_* Z_i]^{1/3} \tag{40}$$

$$\theta_* = (\overline{w\theta})_*/w_*. \tag{41}$$

It must be noted that relation (39.c) has been imposed to simulate the effect of the splattering of the big eddies at the surface that produces a randomly sheared boundary layer with high values of the horizontal velocity variance $\overline{u^2}$. Although expression (39.c) cannot be derived from a similarity analysis, it is nonetheless confirmed by observations and LES results (see Andre et al. 1976). The center of the first grid was chosen to coincide with the surface. Relations (39) are imposed at the upper boundary of this grid, while at the lower boundary (which is then below the surface), the same values are imposed so as to ensure zero derivative of the second-order moments at the surface (consequently, the third-order moments vanish at the surface). Equations (39) specify initial conditions to start the solutions. These presuppose a strong inversion lid and local similarity in the sense that in the M–O similarity the surface heat flux $\overline{w\theta}_0$ is replaced by the local value $\overline{w\theta} = \overline{w\theta}_0(1 - z/h)$. This is not necessarily consistent with the boundary conditions at the surface, but this is irrelevant since the computed mixed layer becomes independent of the initial conditions after about a time $\approx h/w_*$.

At the upper boundary, sufficiently far from the inversion layer ($z \approx 2Z_i$), all turbulent quantities are taken to be zero. The explicit time integration requires a parabolic stability condition, which in principle should be determined by the maximum value of the diffusivities (30) or (36)–(38). Since there is more than one diffusivity, the process of finding the stability condition turns out to be cumbersome and time consuming. We have found, however, that a simpler global criterion can be adopted that reads

$$w_* Z_i \frac{\Delta t}{(\Delta z)^2} < 0.02. \tag{42}$$

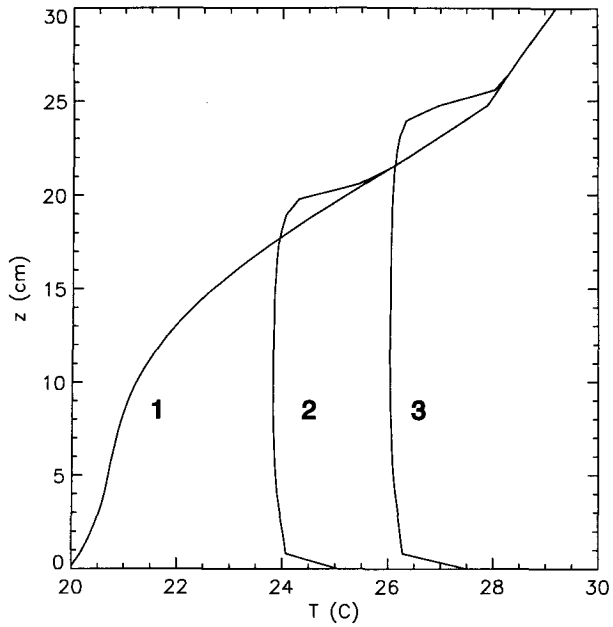


FIG. 1. Profile of the temperature as given by the complete model corresponding to (a) initial time, $t = 0$, (b) $t = 300$ s, and (c) $t = 599$ s.

The initial conditions correspond to zero turbulent variables and a strongly stable temperature profile provided by the experimental set up of Deardorff and Willis (1985). Moreover,

$$\lambda = 0.225 \text{ cm s}^{-2} \text{ K}^{-1}$$

$$(\overline{w\theta})_* = 0.14 \text{ K cm s}^{-1}. \quad (43)$$

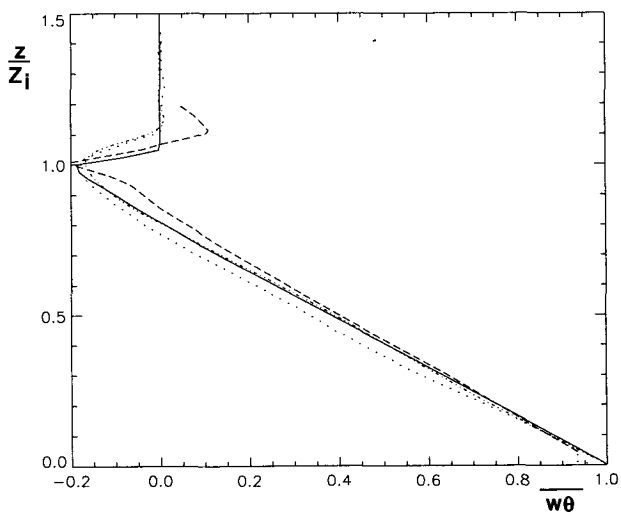


FIG. 2. Profile of the convective heat flux $\overline{w\theta}$ normalized to the heat flux at the bottom $(\overline{w\theta})_*$, Eq. (43). Solid line: complete SOC model, dotted line: Schumann's LES, dashed line: Moeng and Wyngaard's LES, and dash–dotted line: Nieuwstadt's LES.

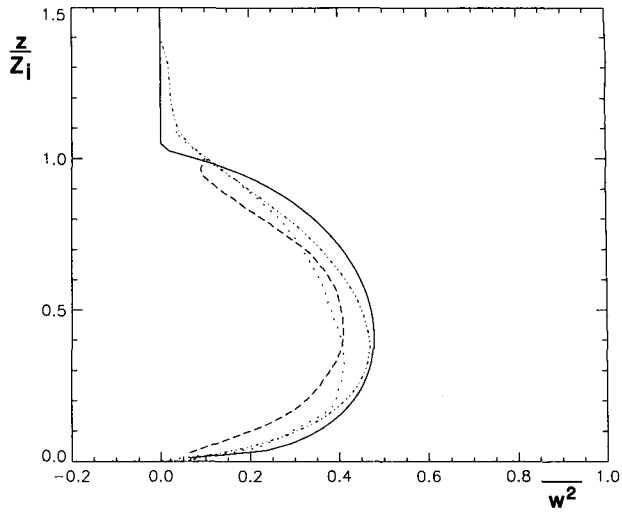


FIG. 3. Turbulent vertical velocity variance $\overline{w^2}$ normalized to $w_*^2$ [see Eq. (40)]. Solid line: complete SOC model, dotted line: Schumann's LES, dashed line: Moeng and Wyngaard's LES, and dash–dotted line: Nieuwstadt's LES.

In Fig. 1 the initial temperature profile is shown, together with those corresponding to $t = 599$ sec and an intermediate time. Our results are very close to those shown in Fig. 1 of Finger and Schmidt (1986), which, in turn, are good representations of the values observed in the experiment by Deardorff and Willis (1985). The resulting second- and third-order moments and the dissipation rates $\epsilon$ and $\epsilon_\theta$ are shown in Figs. 2–13 for the complete model and in Figs. 13–23 for ZL's model, where we also plot the corresponding LES results.

As can be seen, both models yield results in agreement with LES data; the main difference between them

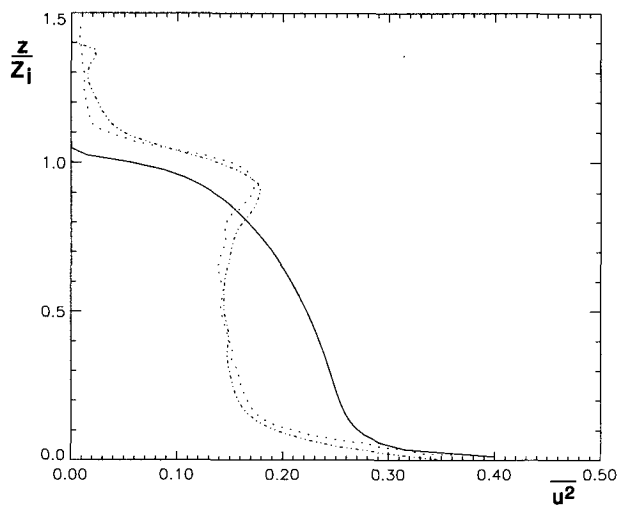


FIG. 4. Profile of the horizontal velocity variance $\overline{u^2}$ normalized to $w_*^2$. Solid line: complete SOC model, dotted line: Schumann's LES, and dash–dotted line: Nieuwstadt's LES.

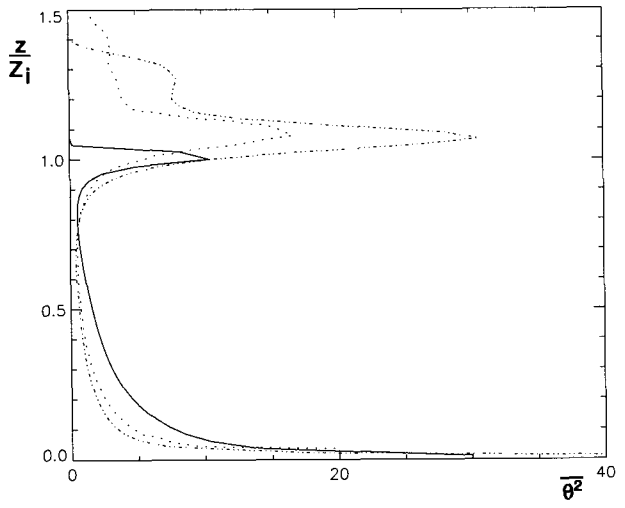


FIG. 5. Profile of the temperature fluctuation variance $\overline{\theta^2}$ normalized to $\theta_*^2$ [see Eq. (41)]. Solid line: complete SOC model, dotted line: Schumann's LES, and dash–dotted line: Nieuwstadt's LES.

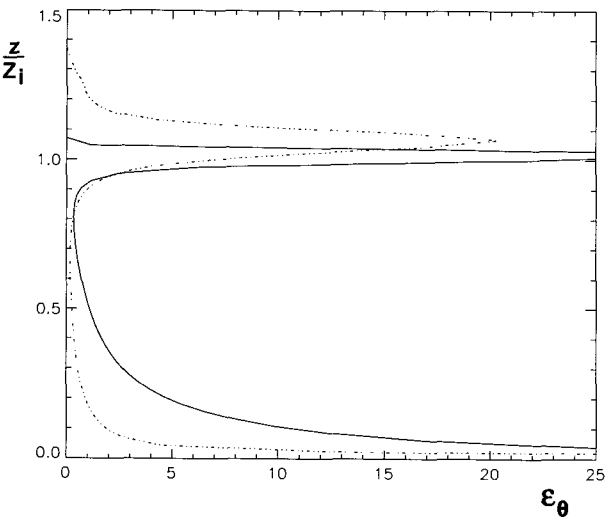


FIG. 7. Profile of the destruction of temperature variance $\epsilon_\theta$ normalized to $w_*\theta_* Z_i^{-1}$. Solid line: complete SOC model, and dash–dotted line: Nieuwstadt's LES.

is that, above the inversion, the LES results show more pronounced features and a slower decay of the magnitudes involving correlations with temperature fluctuations, which are better reproduced by the complete model. The second-order moments are, in general, in very good agreement with the only exception of the horizontal velocity covariance $\overline{u^2}$. According to the LES results, $\overline{u^2}$ shows a secondary maximum near the inversion layer that the SOC models are unable to reproduce. The reason is that, when encountering the capping inversion (or the surface), the eddies splatter and produce a randomly sheared horizontal layer with anomalously high values of $\overline{u^2}$, even quite deeply inside the inversion layer. This effect, which is not captured by the SOC models since they assume zero shear everywhere, can only be accounted for at the surface by imposing the boundary condition (39.c). There is, however, no simple way to impose an analogous condition at the inversion layer, except through modifying the modeled pressure gradient term such as $\Pi_{33}$, Eq. (7). It should be noted that expression (12) does partially account for the splattering effect at the inversion layer:

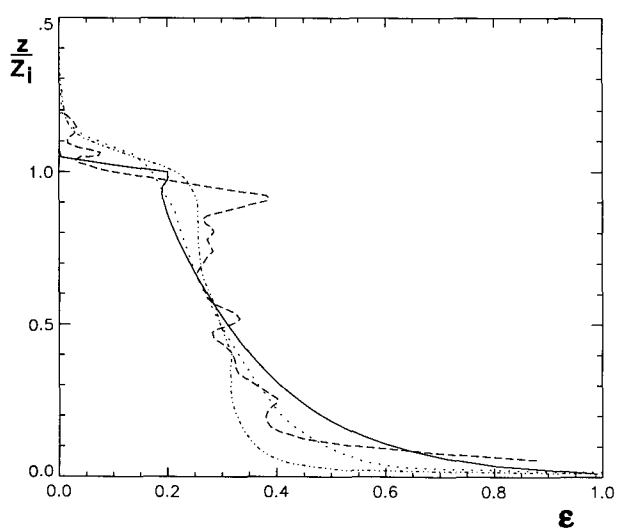


FIG. 6. Profile of the turbulent kinetic energy dissipation $\epsilon$ normalized to $w_*^3 Z_i^{-1}$. Solid line: complete SOC model, dotted line: Schumann's LES, dashed line: Moeng and Wyngaard's LES, and dash–dotted line: Nieuwstadt's LES.

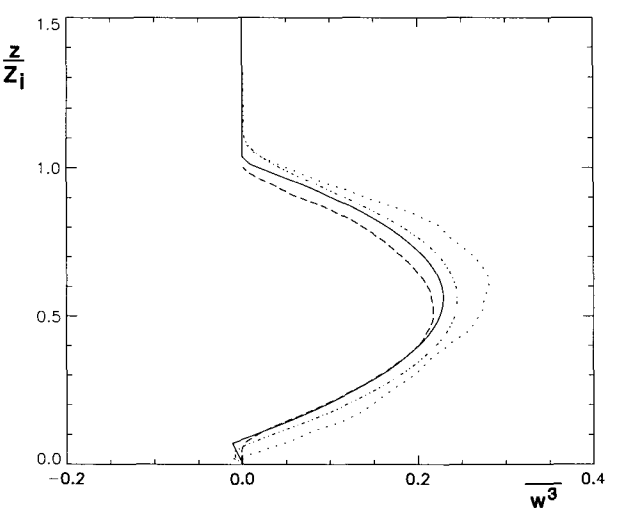


FIG. 8. Profile of the vertical flux of the vertical component of turbulent kinetic energy $\overline{w^3}$ normalized to $w_*^3$. Solid line: complete SOC model, dotted line: Schumann's LES, dashed line: Moeng and Wyngaard's LES, and dash–dotted line: Nieuwstadt's LES.

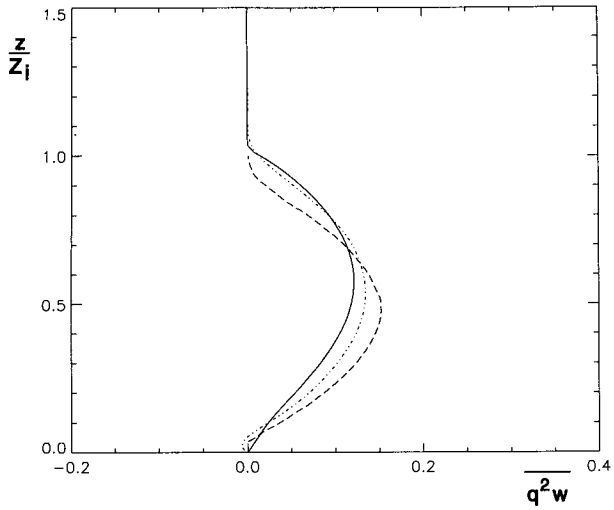


FIG. 9. Profile of the vertical flux of turbulent kinetic energy $\frac{1}{2}\overline{q^2 w}$ normalized to $w_*^3$. Solid line: complete SOC model, dashed line: Moeng and Wyngaard's LES, and dash–dotted line: Nieuwstadt's LES.

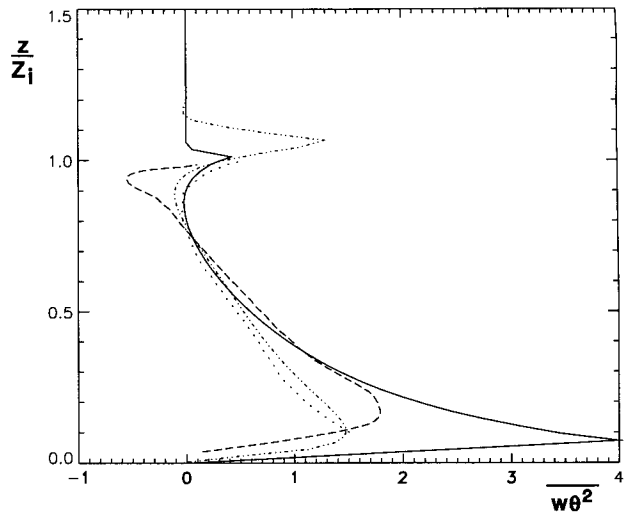


FIG. 11. Profile of the vertical flux of the square of temperature fluctuations $\overline{w\theta^2}$ (proportional to the vertical flux of potential energy) normalized to $w_*\theta_*^2$. Solid line: complete SOC model, dotted line: Schumann's LES, dashed line: Moeng and Wyngaard's LES, and dash–dotted line: Nieuwstadt's LES.

as the Brunt–Väisälä frequency $N$ increases near the inversion layer, $\tau_p$ decreases with respect to the turbulence (decay) time scale $\tau$, and the rate of energy transfer from the vertical to horizontal components is thus enhanced. In fact, use of Eq. (12) considerably improves the behavior of $\overline{u^2}$, which would otherwise decay too fast as the inversion is approached. The splattering effect might also be responsible for the relatively high values of the dissipation $\epsilon$ at and above the inversion layer exhibited by the LES data, a result that cannot be reproduced by the SOC models, even though the predicted $\epsilon$ is in better accord with the LES data than $\overline{u^2}$. As far as the third-order moments are concerned, the overall agreement between LES and SOC results is quite satisfactory, except for the overestimation of $\overline{w\theta^2}$ below $0.1z_i$, a problem that was also reported by Andre (1982). In general, the third-order moments behave correctly both near the ground and in the mixed layer, but fall usually short of the LES values at the inversion layer, although not dramatically. This problem can be traced to the fact that the turbulence time

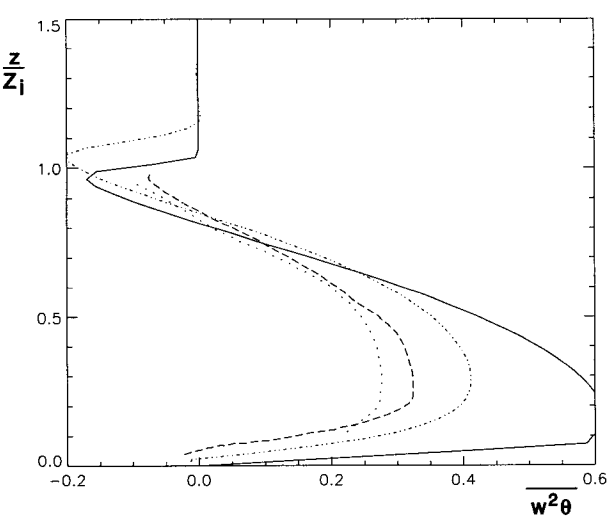


FIG. 10. Profile of the vertical flux of turbulent convective flux $\overline{w^2\theta}$ normalized to $w_*^2\theta_*$. Solid line: complete SOC model, dotted line: Schumann's LES, dashed line: Moeng and Wyngaard's LES, and dash–dotted line: Nieuwstadt's LES.

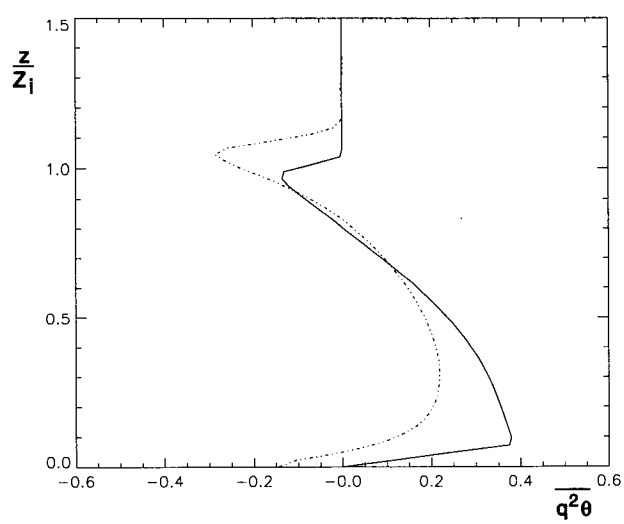


FIG. 12. Profile of the triple correlation between temperature fluctuations and turbulent kinetic energy $\frac{1}{2}\overline{q^2\theta}$ normalized to $w_*^2\theta_*$. Solid line: complete SOC model, and dash–dotted line: Nieuwstadt's LES.

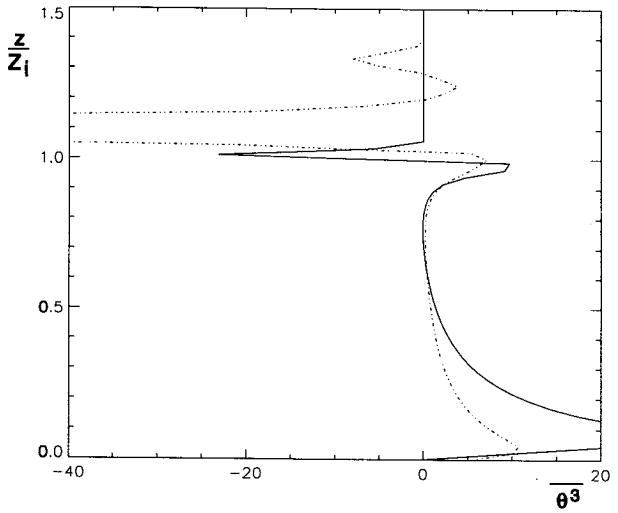


FIG. 13. Profile of the triple correlation of temperature fluctuations $\overline{\theta^3}$ normalized to $\theta_*^3$. Solid line: complete SOC model, and dash–dotted line: Nieuwstadt's LES.

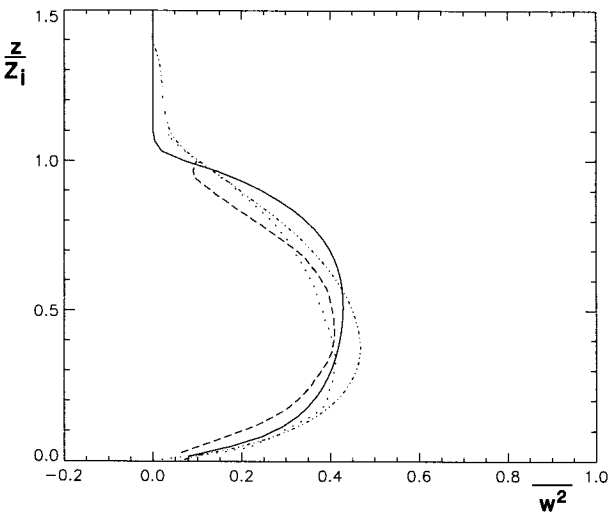


FIG. 15. Turbulent vertical velocity variance $\overline{w^2}$ normalized to $w_*^2$ [see Eq. (40)]. Solid line: ZL SOC model, dotted line: Schumann's LES, dashed line: Moeng and Wyngaard's LES, and dash–dotted line: Nieuwstadt's LES.

scale $\tau$ is unrealistically small due to the rapid decrease of turbulent kinetic energy in the inversion layer as compared with the LES results (also related to the unrealistic profile of $\overline{u^2}$ near the inversion layer). Since the third-order moment time scale that controls the return-to-isotropy effect, $\tau_3$, is taken proportional to $\tau$, an unrealistically small $\tau$ overestimates the relaxation and, consequently, produces very low third-order moments. This effect can be partially corrected in the complete SOC model by decreasing the value of the constant $c_8$ so as to increase the effective value of $\tau_3$. In this way, a better agreement between the results of the complete SOC model and the LES data at the inversion layer is achieved and, as a bonus, a more realistic profile of $\theta^2$, with a more pronounced peak at the inversion layer, is also obtained. This is the reason we have chosen the value of $c_8$ to be 7.0 instead of the value of 8.0 quoted in the literature (Andre et al. 1982).

In general, while the performance of the complete SOC model versus the ZL model when compared with the LES data may be a matter of personal judgment, we have found that there is an important difference.

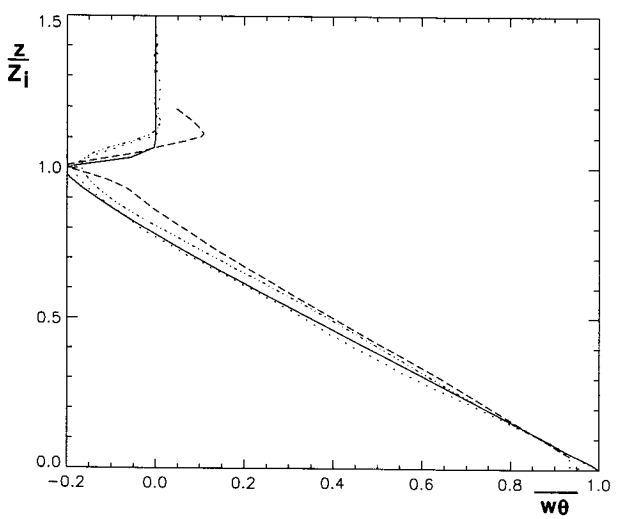


FIG. 14. Profile of the convective heat flux $\overline{w\theta}$ normalized with the heat flux at the bottom $(\overline{w\theta})_*$, Eq. (43). Solid line: ZL SOC model, dotted line: Schumann's LES, dashed line: Moeng and Wyngaard's LES, and dash–dotted line: Nieuwstadt's LES.

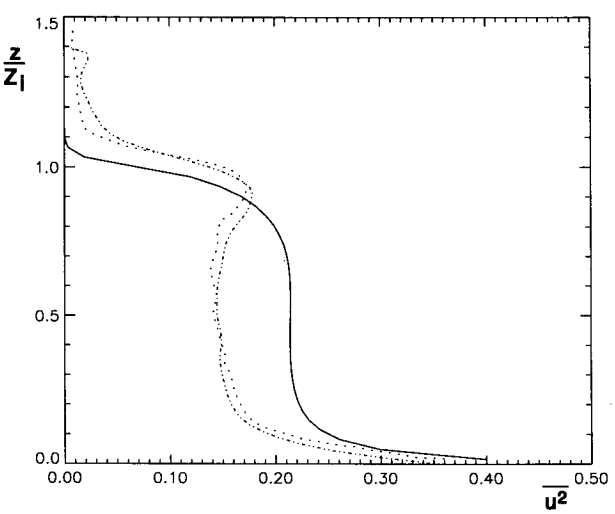


FIG. 16. Profile of the horizontal velocity variance $\overline{u^2}$ normalized to $w_*^2$. Solid line: ZL SOC model, dotted line: Schumann's LES, and dash–dotted line: Nieuwstadt's LES.

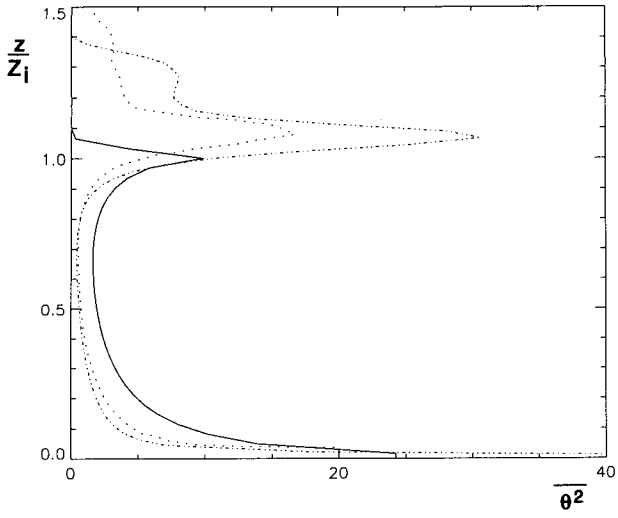


FIG. 17. Profile of the temperature fluctuation variance $\overline{\theta^2}$ normalized to $\theta_*^2$. Solid line: ZL SOC model, dotted line: Schumann's LES, and dash–dotted line: Nieuwstadt's LES.

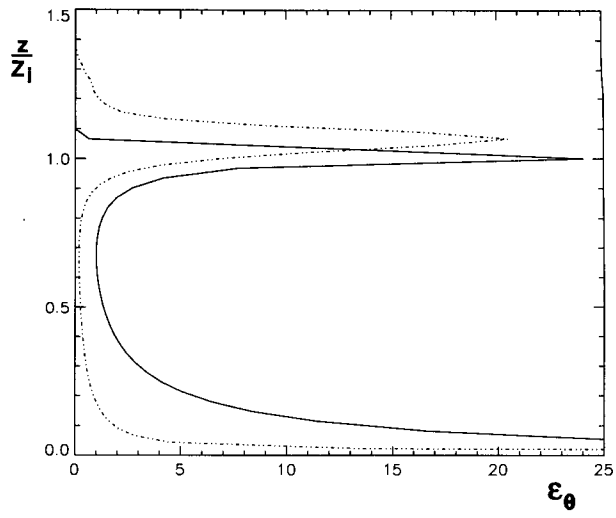


FIG. 19. Profile of the destruction of temperature variance $\epsilon_\theta$ normalized to $w_*\theta_* Z_i^{-1}$. Solid line: ZL SOC model, and dash–dotted line: Nieuwstadt's LES.

The ZL model is much more *sensitive to the value of the model constants* of the third-order moment equations than the SOC model. For example (see next section), increasing $\mu$ by 20% produces changes in the values of the third-order moments at the center of the mixed layer ranging from 60% to 94%, while the most sensitive constant of the complete model, $c_8$, when incremented by 20% produces changes in the third-order moments at the same point between 9% and 17.6%. The changes produced by a 20% increase of $c_{10}$ and $c_{11}$ are below 7% and 3%, respectively. This robustness makes the complete model better suited for predictive calculations under more general conditions.

## 8. Model constants and sensitivity study

The values chosen for the constants of the model are as follows:

$$c_2 = 1, \quad c_4 = 1.75, \quad c_5 = 0.3, \quad c_6 = 3.25,$$

$$c_7 = \frac{1}{2}, \quad a = 0.1, \quad a_1 = 0.95, \quad a_2 = 3.8,$$

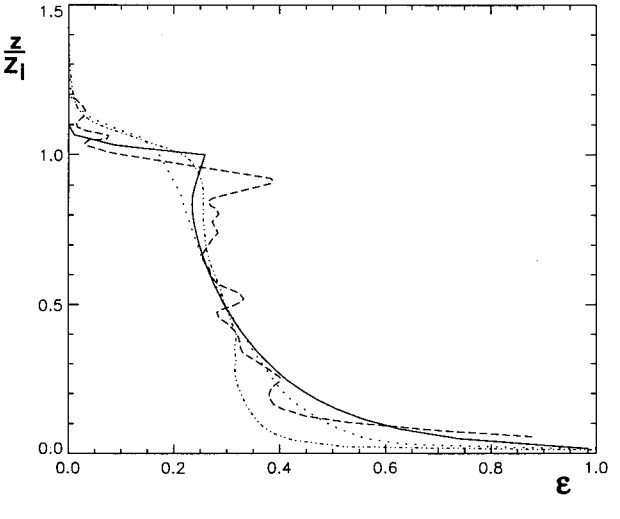


FIG. 18. Profile of the turbulent kinetic energy dissipation $\epsilon$ normalized to $w_*^3 Z_i^{-1}$. Solid line: ZL SOC model, dotted line: Schumann's LES, dashed line: Moeng and Wyngaard's LES, and dash–dotted line: Nieuwstadt's LES.

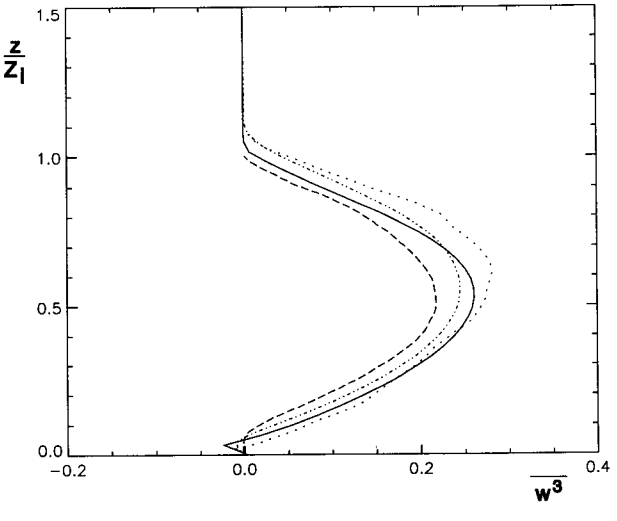


FIG. 20. Profile of the vertical flux of the vertical component of turbulent kinetic energy $\overline{w^3}$ normalized to $w_*^3$. Solid line: ZL SOC model, dotted line: Schumann's LES, dashed line: Moeng and Wyngaard's LES, and dash–dotted line: Nieuwstadt's LES.

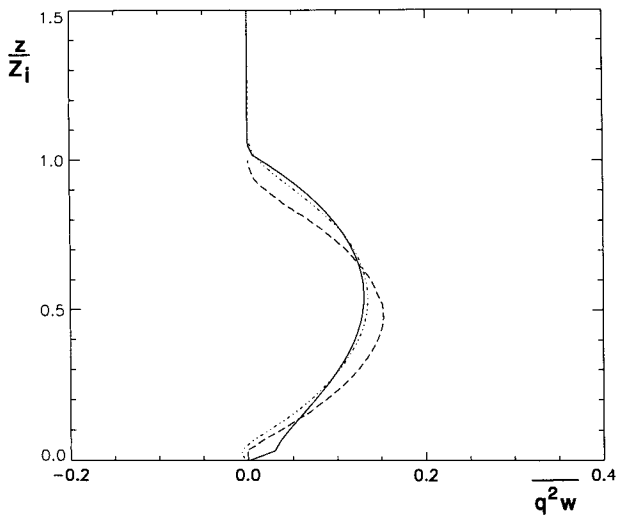


FIG. 21. Profile of the vertical flux of turbulent kinetic energy $\frac{1}{2}\overline{q^2 w}$ normalized to $w_*^3$. Solid line: ZL SOC model, dashed line: Moeng and Wyngaard's LES, and dash–dotted line: Nieuwstadt's LES.

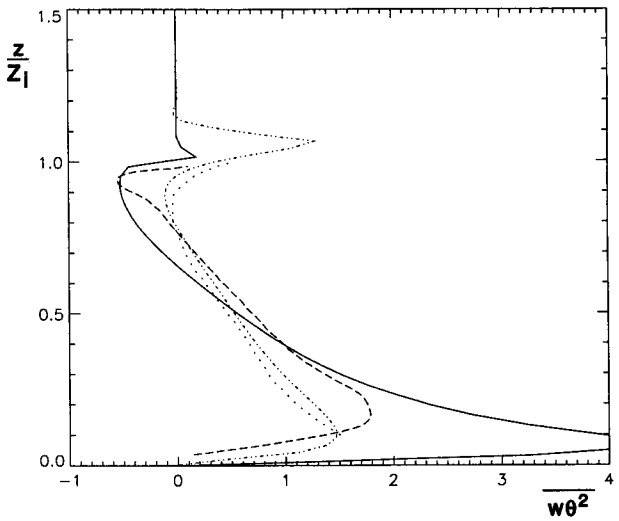


FIG. 23. Profile of the vertical flux of the square of temperature fluctuations $\overline{w\theta^2}$ (proportional to the vertical flux of potential energy) normalized to $w_*\theta_*^2$. Solid line: ZL SOC model, dotted line: Schumann's LES, dashed line: Moeng and Wyngaard's LES, and dash–dotted line: Nieuwstadt's LES.

$$c_* = 0, \quad c_8 = 7, \quad c_{10} = 4, \quad c_{11} = \frac{1}{5},$$

$$A_0 = 0.075. \tag{44}$$

The constants in the second-order equations have standard values (Zeman and Lumley 1979) except for $c_7$, whose value we take to be $1/2$ (Moeng and Wyngaard 1986), rather than the isotropic value $1/3$.

We have studied the sensitivity of the model with respect to changes of the model constants in the third-order moment equations by monitoring the ensuing variations of the third-order moments at the midpoint of the convective layer. In the case of the complete SOC model we have varied the constants $c_8$, $c_{10}$, and $c_{11}$, while only $\mu$ was changed in the case of ZL's model. In all cases the constants have been increased by 20% of the reported values. The percentile changes in the different third-order moments are summarized in Table 1.

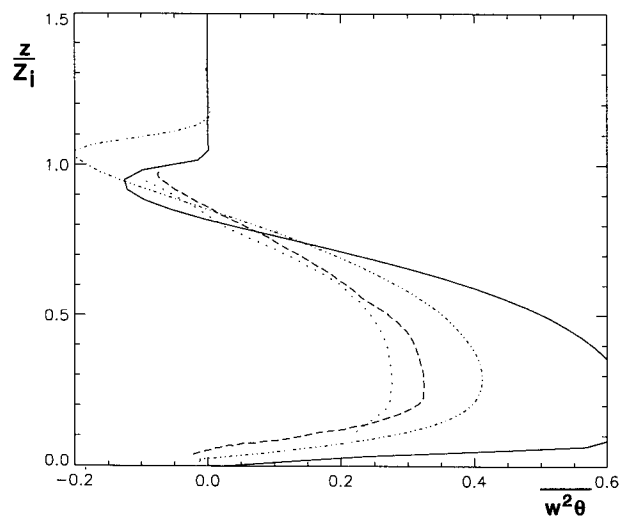


FIG. 22. Profile of the vertical flux of turbulent convective flux $\overline{w^2\theta}$ normalized to $w_*^2\theta_*$. Solid line: ZL SOC model, dotted line: Schumann's LES, dashed line: Moeng and Wyngaard's LES, and dash–dotted line: Nieuwstadt's LES.

As stated in section 2, that we did not assume that the time scale entering the pressure velocity and pressure temperature correlations, Eqs. (10)–(11), is equal to the eddy turnover time $\tau$ has helped improve the SOC results. To make the point more quantitative, in Figs. 24–25 we plot $\overline{u^2}$ and the dissipation $\epsilon$ resulting from the assumption $\tau_p = \tau$. Comparison with Figs. 4 and 6 shows that Eq. (12) does indeed have a significant effect in the stably stratified region by bringing the results closer to the LES values.

## 9. Conclusions

In this paper we have presented a new set of equations for the third-order moments in terms of the sec-

TABLE 1.

| +20% | $c_8$ | $c_{10}$ | $c_{11}$ | $\mu$ (ZL) |
|---|---|---|---|---|
| $\overline{w^3}$ | −17.6% | +6.3% | −2.6% | +65% |
| $\overline{q^2 w}$ | −15.3% | +6.5% | −1.9% | +62% |
| $\overline{w^2\theta}$ | −16.9% | +5.8% | +0.16% | +60% |
| $\overline{w\theta^2}$ | −9.0% | +6.7% | +0.27% | +94% |

ond-order moments. The results obtained with these equations compare well with LES simulations. We have also found that expression (12) for the return-to-isotropy time scale in the presence of stable stratification greatly improves the results of both versions of the SOC model, which suggests that further improvements could be achieved by a better modeling of the pressure terms, possibly using some nonlocal expressions that have been shown to be very successful in the case of shear flows (Durbin 1993). For most applications, however, we believe that the SOC model presented here gives results comparable to those obtained with LES codes and should thus be used to replace past SOC models. In addition, it is argued that the poor representation of the splattering effect near the inversion layer might be the cause of the failure of most SOC models in reproducing the observed features in that layer.

We have also presented a comparison with the original version of ZL's third-order moment equations. It is remarkable that this relatively simple model compares so well with the LES data and this fact demands an explanation. First, as mentioned earlier, a substantial improvement has been achieved by incorporating expression (12). Further improvements are due to the new dissipation equation, Eq. (13), which contains a Brunt–Väisälä frequency $N$ term that accounts for the effect of $N$ on the turbulence length scale. Application of boundary conditions to all second-order quantities in agreement with observations and LES results near the lower boundary also improved the performances of both SOC models.

In conclusion, it may be said that the present model contains more terms in the expansion for the individual third-order moments, which makes it more robust or less sensitive to changes in the value of the model constants. On the other hand, the ZL model is apparently a truncated version of the present model, and the discarded higher-order terms (such as those containing temperature gradients) are absorbed in the model constants, making the ZL model less robust than its complete counterpart. Still, the present results suggest that the ZL model contains the essential physics of the third-order transport and of the buoyancy-driven flows in general.

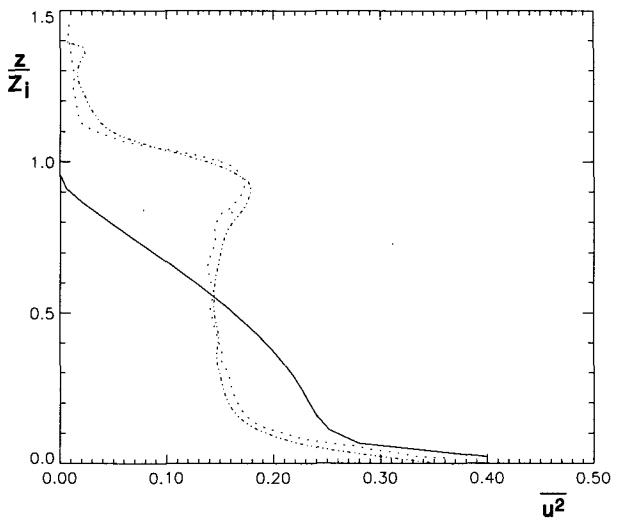


FIG. 24. Profile of the horizontal velocity variance $\overline{u^2}$ normalized to $w_*^2$ *under the assumption* that $\tau_p = \tau$. Solid line: complete SOC model, dotted line: Schumann's LES, and dash–dotted line: Nieuwstadt's LES. As one can notice, the agreement with the LES data is considerably less satisfactory than that of Fig. 4 corresponding to the use of Eq. (12).

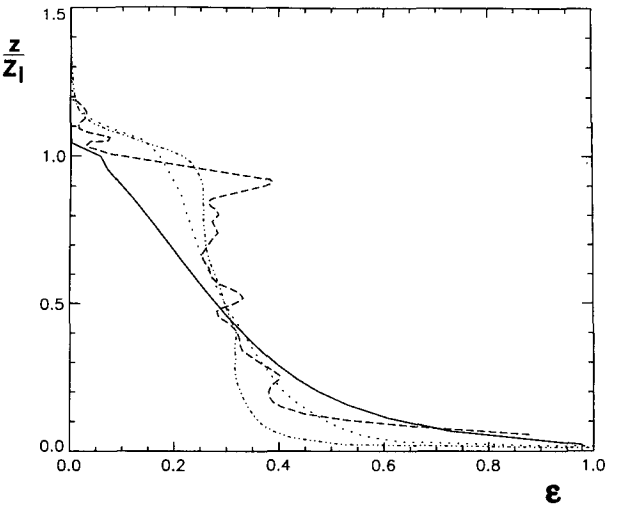


FIG. 25. Same as in Fig. 24 for the dissipation $\epsilon$.

*Acknowledgments.* VMC would like to thank Dr. C. H. Moeng for providing the third-order LES results and MY would like to thank Prof. F. T. M. Nieuwstadt for the use of his LES code. FM would like to thank CONICET (The Consejo de Investigaciones Cientificas y Tecnicas of Argentina) for a postdoctoral fellowship at the Goddard Institute for Space Studies (NASA).

## APPENDIX

### The Turbulent Viscosities (Diffusivities)

Each of the diffusivities $A_k, \ldots, F_k$ has the form exhibited in (30). Furthermore, each $A_{k1}, A_{k2}, \ldots, F_{k1}, F_{k2}$ has the form

$$\Delta A_{11} = A_{110} + A_{111}x + A_{112}x^2 + A_{113}x^3 \quad \text{(A1)}$$

$$\Delta A_{12} = A_{120} + A_{121}x + A_{122}x^2 + A_{123}x^3. \quad \text{(A2)}$$

etc.

The only exception is $F_{21}$, which has an additional $x^4$. Since (71)–(76) arise from the inversion of a matrix, there is a denominator $\Delta$ whose structure is

$$\Delta = \Delta_0 + \Delta_1 x + \Delta_2 x^2 + \Delta_3 x^3, \quad \text{(A3a)}$$

where the coefficients $\Delta_i$ depend on the model constants only, and the dimensionless function $x$ is defined as

$$x \equiv g\alpha\beta\tau^2. \tag{A3b}$$

Using the coefficients $c$'s given in section 8, namely,

$$c_8 = 7, \quad c_{10} = 4, \quad c_{11} = \frac{1}{5}, \quad c_* = 0, \quad c_2 = 1, \tag{A4}$$

we have obtained the following numerical values:

$$\Delta_0 = 6.85 \times 10^6, \quad \Delta_1 = -3.08 \times 10^5,$$
$$\Delta_2 = 2.30 \times 10^3, \quad \Delta_3 = -4.61 \tag{A5}$$

$A_{110} = -9.7843 \times 10^5$ $A_{111} = 1.9994 \times 10^4$
$A_{112} = -61.44$ $A_{113} = 0$

$A_{120} = -9.4219 \times 10^4$ $A_{121} = 361.81$
$A_{122} = 0$ $A_{123} = 0$

$A_{210} = 0$ $A_{211} = -9.6768 \times 10^4$
$A_{212} = 1.9584 \times 10^3$ $A_{213} = -5.76$

$A_{220} = -4.8922 \times 10^5$ $A_{221} = 9.7664 \times 10^3$
$A_{222} = -26.88$ $A_{223} = 0$

$A_{310} = -4.7111 \times 10^4$ $A_{311} = 180.91$
$A_{312} = 0$ $A_{313} = 0$

$A_{320} = -1.4133 \times 10^4$ $A_{321} = 54.272$
$A_{322} = 0$ $A_{323} = 0$

$A_{410} = 0$ $A_{411} = 4.0320 \times 10^3$
$A_{412} = -67.2$ $A_{413} = 0$

$A_{420} = 0$ $A_{421} = 230.40$ $A_{422} = -3.84$ $A_{423} = 0$

$B_{110} = -1.4838 \times 10^5$ $B_{111} = 3.0396 \times 10^3$
$B_{112} = -9.216$ $B_{113} = 0$

$B_{120} = -1.4193 \times 10^4$ $B_{121} = 53.248$
$B_{122} = 0$ $B_{123} = 0$

$B_{210} = -1.3548 \times 10^6$ $B_{211} = 4.6054 \times 10^4$
$B_{212} = -147.20$ $B_{213} = 0$

$B_{220} = -7.7414 \times 10^4$ $B_{221} = 1.6179 \times 10^3$
$B_{222} = -4.608$ $B_{223} = 0$

$B_{310} = -7.0963 \times 10^3$ $B_{311} = 26.624$
$B_{312} = 0$ $B_{313} = 0$

$B_{320} = -2.1289 \times 10^3$ $B_{321} = 7.9872$
$B_{322} = 0$ $B_{323} = 0$

$B_{410} = 5.6448 \times 10^4$ $B_{411} = -1.7173 \times 10^3$
$B_{412} = 0$ $B_{413} = 0$

$B_{420} = 3.2256 \times 10^3$ $B_{421} = -98.133$
$B_{422} = 0$ $B_{423} = 0$

$C_{110} = 0$ $C_{111} = -1.0871 \times 10^5$
$C_{112} = 409.6$ $C_{113} = 0$

$C_{120} = -7.6100 \times 10^5$ $C_{121} = 1.1110 \times 10^4$
$C_{122} = -30.72$ $C_{123} = 0$

$C_{210} = 0$ $C_{211} = 0$ $C_{212} = -1.0752 \times 10^4$
$C_{213} = 38.4$

$C_{220} = 0$ $C_{221} = -5.4357 \times 10^4$
$C_{222} = 179.2$ $C_{223} = 0$

$C_{310} = -3.8050 \times 10^5$ $C_{311} = 5.5552 \times 10^3$
$C_{312} = -15.36$ $C_{313} = 0$

$C_{320} = -1.1415 \times 10^5$ $C_{321} = 1.6666 \times 10^3$
$C_{322} = -4.608$ $C_{323} = 0$

$C_{410} = 0$ $C_{411} = 0$ $C_{412} = 448$ $C_{413} = 0$

$C_{420} = 0$ $C_{421} = 0$ $C_{422} = 25.6$ $C_{423} = 0$

$D_{110} = -9.7843 \times 10^5$ $D_{111} = 1.8844 \times 10^4$
$D_{112} = -76.8$ $D_{113} = 0$

$D_{120} = -1.0871 \times 10^5$ $D_{121} = 607.57$
$D_{122} = 0$ $D_{123} = 0$

$D_{210} = 0$ $D_{211} = -5.6448 \times 10^4$
$D_{212} = 181.33$ $D_{213} = 0$

$D_{220} = 0$ $D_{221} = -1.0991 \times 10^4$
$D_{222} = 53.76$ $D_{223} = 0$

$D_{310} = -5.4357 \times 10^4$ $D_{311} = 303.79$
$D_{312} = 0$ $D_{313} = 0$

$D_{320} = -1.6307 \times 10^4$ $D_{321} = 91.136$
$D_{322} = 0$ $D_{323} = 0$

$D_{410} = 0$ $D_{411} = -2.8224 \times 10^4$
$D_{412} = 1.2683 \times 10^3$ $D_{413} = -5.76$

$D_{420} = -4.8922 \times 10^5$ $D_{421} = 2.0413 \times 10^4$
$D_{422} = -92.16$ $D_{423} = 0$

$E_{110} = -1.3548 \times 10^5$ $E_{111} = 2.7153 \times 10^3$
$E_{112} = -9.216$ $E_{113} = 0$

$E_{120} = -1.3715 \times 10^4$ $E_{121} = 61.44$
$E_{122} = 0$ $E_{123} = 0$

$$E_{210} = -7.9027 \times 10^5 \quad E_{211} = 2.4043 \times 10^4$$
$$E_{212} = -76.8 \quad E_{213} = 0$$
$$E_{220} = -4.5158 \times 10^4 \quad E_{221} = 394.24$$
$$E_{222} = 0 \quad E_{223} = 0$$
$$E_{310} = -6.88574 \times 10^3 \quad E_{311} = 30.72$$
$$E_{312} = 0 \quad E_{313} = 0$$
$$E_{320} = -2.0572 \times 10^3 \quad E_{321} = 9.216$$
$$E_{322} = 0 \quad E_{323} = 0$$
$$E_{410} = -3.9514 \times 10^5 \quad E_{411} = 1.6860 \times 10^4$$
$$E_{412} = -80.64 \quad E_{413} = 0$$
$$E_{420} = -2.2579 \times 10^4 \quad E_{421} = 936.41$$
$$E_{422} = -4.608 \quad E_{423} = 0$$
$$F_{110} = 0 \quad F_{111} = 0 \quad F_{112} = -4.0768 \times 10^4$$
$$F_{113} = 153.6$$
$$F_{120} = 0 \quad F_{121} = -2.8538 \times 10^5$$
$$F_{122} = 4.1664 \times 10^3 \quad F_{123} = -11.52$$
$$F_{210} = 0 \quad F_{211} = 0 \quad F_{212} = 0$$
$$F_{213} = -4.0320 \times 10^3 \quad F_{214} = 14.41$$
$$F_{220} = 0 \quad F_{221} = 0 \quad F_{222} = -2.0384 \times 10^4$$
$$F_{223} = 67.2$$
$$F_{310} = 0 \quad F_{311} = -1.4269 \times 10^5$$
$$F_{312} = 2.0832 \times 10^3 \quad F_{313} = -5.76$$
$$F_{320} = -2.5684 \times 10^6 \quad F_{321} = 7.2830 \times 10^4$$
$$F_{322} = -239.36 \quad F_{323} = 0$$
$$F_{410} = 0 \quad F_{411} = 0 \quad F_{412} = 0 \quad F_{413} = 168$$
$$F_{420} = 0 \quad F_{421} = 0 \quad F_{422} = 0 \quad F_{423} = 9.6.$$

## REFERENCES


Andre, J. C., G. De Moor, P. Lacarrere, and R. du Vachat, 1976: Turbulence approximation for inhomogeneous flows: Part II. The numerical simulation of a penetrative convection experiment. *J. Atmos. Sci.*, **33,** 482–491.

——, ——, ——, G. Therry, and R. Du Vachat, 1978: Modeling the 24-h evolution of the mean and turbulent structure of the planetary boundary layer. *J. Atmos. Sci.*, **35,** 1861–1883.

——, P. Lacarrere, and K. Traore, 1982: Pressure effects on triple correlations in turbulent convective flows. *Turbulent Shear Flow.* Vol. 3. Springer, 243–252.

Bougeault, P., 1981: Modeling the trade-wind cumulus boundary layer. Part II: A high-order one-dimensional model. *J. Atmos. Sci.*, **38,** 2429–2439.

——, and J. C. Andre, 1986: On the stability of the third-order turbulence closure for the modeling of the stratocumulus-topped boundary layer. *J. Atmos. Sci.*, **43,** 1574–1581.

Canuto, V. M., 1992: Turbulent convection with overshooting: Reynolds stress approach. *Astrophys. J.*, **392,** 218–232.

——, and F. Minotti, 1993: Stratified turbulence in the atmosphere and oceans: A new subgrid model. *J. Atmos. Sci.*, **50,** 1925–1935.

Chen, C., and W. R. Cotton, 1983: Numerical experiments with a one-dimensional higher order turbulence model: Simulation of the Wangara day 33. *Bound.-Layer Meteor.*, **32,** 205–306.

Clarke, R. H., A. J. Dyer, R. R. Brook, D. G. Reid, and A. J. Troup, 1971: The Wangara Experiment: Boundary layer data. Tech. Paper 19, Div. Meteor. Phys., CSIRO, Australia, 316 pp.

Deardorff, J. W., and G. E. Willis, 1985: Further results from a laboratory model of the convective planetary boundary layer. *Bound.-Layer Meteor.*, **32,** 205–236.

Durbin, P. A., 1993: A Reynolds stress model for near-wall turbulence. *J. Fluid Mech.*, **249,** 465–498.

Finger, J. E., and H. Schmidt, 1986: On the efficiency of different higher order turbulence models simulating the convective boundary layer. *Beitr. Phys. Atmos.*, **59,** 505–517.

Hanjalic, K., and B. E. Launder, 1972: A Reynolds stress model of turbulence and its application to thin shear flow. *J. Fluid Mech.*, **52,** 609–638.

——, and ——, 1976: Contribution towards a Reynolds stress closure for low Reynolds number turbulence. *J. Fluid Mech.*, **74,** 593–610.

Holt, S. E., J. R. Koseff, and J. H. Ferziger, 1992: A numerical study of the evolution and structure of homogeneous stably stratified sheared turbulence. *J. Fluid Mech.*, **237,** 499–539.

Lumley, J. L., 1978: Computational modeling of turbulent flows. *Advances in Applied Mechanics,* Vol. 18, Academic Press, 123–176.

——, O. Zeman, and J. Siess, 1978: The influence of buoyancy on turbulent transport. *J. Fluid Mech.*, **84,** 581–597.

Moeng, C. H., and J. C. Wyngaard, 1986: An analysis of closures for pressure-scalar covariances in the convective boundary layer. *J. Atmos. Sci.*, **43,** 2499–2513.

——, and ——, 1989: Evaluation of turbulent transport and dissipation closures in second-order modeling. *J. Atmos. Sci.*, **46,** 2311–2330.

Nieuwstadt, F. T. M., and R. Brost, 1986: Decay of convective turbulence. *J. Atmos. Sci.*, **43,** 532–546.

——, P. J. Mason, C.-H. Moeng, and U. Schumann, 1993: Large-eddy simulation of the convective boundary layer: A comparison of four computer codes. *Turbulent Shear Flows,* Vol. 8, F. Durst et al., Eds., Springer-Verlag, 431 pp.

Shih, T.-H., and J. L. Lumley, 1985: *Modeling of Pressure Correlation Terms in Reynolds Stress and Scalar Flux Equations.* Cornell University, FDA-85-3.

——, and A. Shabbir, 1992: Advances in modeling the pressure correlation terms in the second moment equations. *Studies in Turbulence,* Springer-Verlag, 91–128.

Speziale, C. G., 1991: Analytical models for the development of Reynolds stress closures in turbulence. *Ann. Rev. Fluid Mech.*, **23,** 107–157.

Sun, W.-Y., and Y. Ogura, 1980: Modeling the evolution of the convective planetary boundary layer. *J. Atmos. Sci.*, **37,** 1558–1572.

Weinstock, J., 1987: A theory of turbulent transport. *J. Fluid Mech.*, **202,** 319–338.

Willis, G. E., and J. W. Deardorff, 1974: A laboratory model of the unstable planetary boundary layer. *J. Atmos. Sci.*, **31,** 1297–1307.

Wyngaard, J. C., and O. R. Cote, 1975: The evolution of the convective planetary boundary layer—A higher-order closure model study. *Bound.-Layer Meteor.*, **7,** 289–308.

Zeman, O., 1975: The dynamics of entrainment in planetary boundary layers—A study in turbulence modeling and parameterization. Ph.D. thesis, The Pennsylvania State University, University Park, PA 16802.

——, and J. L. Lumley, 1976: Modeling buoyancy driven mixed layers. *J. Atmos. Sci.*, **33,** 1974–1988.

——, and H. Tennekes, 1977: Parameterization of the turbulent energy budget at the top of the daytime atmospheric boundary layer. *J. Atmos. Sci.*, **34,** 111–123.

——, and J. L. Lumley, 1979: *Turbulent Shear Flows.* Vol. 1. Springer, 295 pp.